doi.org/10.36721/PJPS/2026.40.16992.1

Everolimus inhibits mTORC1 signaling, promotes TFEB nuclear translocation and activates ER-phagy in triple-negative breast cancer

Xia Da[1#], Bin Zhang[1#], Jin Lv[2] and Jin Xu[1]*

[1]Department of Thyroid and Breast Surgery, Nanjing First Hospital, Nanjing Medical University, Nanjing, Jiangsu, 210006, China
[2]Department of General Surgery, Nanjing First Hospital, Nanjing Medical University, Nanjing, Jiangsu, 210006, China

Abstract: **Background**: Triple-negative breast cancer (TNBC) is aggressive with a poor prognosis. Everolimus, an mTORC1 inhibitor, shows limited efficacy as monotherapy in TNBC and the mechanisms remain unclear. **Objectives**: This study investigated whether everolimus promotes TFEB nuclear translocation by inhibiting mTORC1, whether nuclear TFEB upregulates the ER-phagy receptors FAM134B, RTN3L and CALCOCO1 and whether FAM134B mediates its anti-TNBC effect. **Methods**: MDA-MB-231 and MDA-MB-468 cells were used. Viability and apoptosis were assessed by CCK-8 and flow cytometry. TFEB nuclear translocation was analyzed by immunofluorescence and nucleocytoplasmic fractionation. Autophagic flux and ER-phagy receptor expression were examined by Western blot and BafA1 blockade. ER-phagy flux was verified by mCherry-GFP-KDEL reporter assay and electron microscopy. ChIP-qPCR validated TFEB-receptor promoter binding. siRNA knockdown and complementation assays determined molecular necessity. In vivo effects were confirmed in xenograft models. **Results**: Everolimus inhibited TNBC cell viability in a dose- and time-dependent manner (72 h inhibition: 77.55%) and induced apoptosis (from 6.2% to 34.7%). Everolimus inhibited mTORC1 signaling, as shown by reduced phosphorylation of S6K and 4E-BP1 and promoted TFEB nuclear translocation (from 8.6% to 76.3%). Nuclear TFEB directly bound to CLEAR elements in the promoters of FAM134B, RTN3L and CALCOCO1, upregulating their expression (FAM134B, 4.32-fold) and driving ER-phagy flux (autophagic vesicles per cell section: 0.34 to 5.68; mCherry/GFP ratio: 0.23 to 0.81). TFEB knockdown blocked these effects and reversed everolimus-induced cytotoxicity. FAM134B knockdown alone reversed everolimus-induced cell death (viability recovered from 22.45% to 78.92% at 72 h) and ER-phagy, whereas FAM134B re-expression restored sensitivity. *In vivo*, everolimus reduced tumor volume by 62.3%, accompanied by enhanced TFEB nuclear translocation, increased FAM134B expression and LC3-II accumulation. **Conclusion**: Everolimus inhibits TNBC by suppressing mTORC1-mediated TFEB phosphorylation, promoting TFEB nuclear translocation and FAM134B upregulation, ultimately inducing lethal ER-phagy. FAM134B is a major downstream effector and candidate efficacy biomarker.

Keywords: Everolimus; Endoplasmic reticulum autophagy; FAM134B; mTORC1 signaling pathway; Triple-negative breast cancer; TFEB nuclear translocation

Submitted 16-06-2026 – Revised 13-08-2026 – Accepted 17-08-2026

Article in Press

INTRODUCTION

Triple-negative breast cancer (TNBC) is the breast cancer subtype with the poorest prognosis. It lacks expression of estrogen receptors, progesterone receptors and HER2 (Soleimani *et al*., 2025; Valachis *et al*., 2026), which severely limits targeted treatment options. Consequently, patients are often diagnosed at an advanced stage and are prone to early recurrence and metastasis.Once metastasis occurs, the median survival is less than 1 year (Polho *et al*., 2025; Rota *et al*., 2025). Although immune checkpoint inhibitors and antibody-drug conjugates have shown promise in some patients, their overall efficacy remains suboptimal.Chemotherapy remains the mainstay of systemic treatment for TNBC, but drug resistance inevitably leads to treatment failure (Nafissi *et al*., 2026; Khadiri *et al*., 2026). Therefore, elucidating the unique survival and stress-adaptive mechanisms of TNBC and identifying new therapeutic targets are essential to improve clinical outcomes.

The endoplasmic reticulum (ER) is a key organelle for protein synthesis, folding and secretion. Because TNBC cells proliferate rapidly and have high genomic instability and metabolic demand, their ER protein load is markedly increased, making them prone to endoplasmic reticulum stress (ERS) (Licata *et al*., 2025). Moderate ERS activates the unfolded protein response and helps cells restore homeostasis, whereas excessive or prolonged stress induces apoptosis (Alkassis *et al*., 2025).. To survive in an unfavorable microenvironment, TNBC cells often develop adaptive mechanisms. Among these, ER-phagy is important for removing damaged ER and alleviating excessive protein load (Zhao *et al*., 2025; Zhang *et al*., 2025a). However, how ERS affects ER-phagy receptor expression through transcriptional regulation to drive treatment resistance remains unclear.Therefore, overactivated ER-phagy may represent an important survival strategy in therapy-resistant TNBC.Recent studies have revealed close relationships between components of the ERS regulatory network and treatment resistance and poor prognosis in TNBC (Wang *et al*., 2025a; Shang *et al*., 2026). However, how ERS affects

**Corresponding author:* e-mail: qpkoij8455126@sina.com
#These authors contributed equally and are the co-first authors.

ER-phagy receptor expression through transcriptional regulation to drive treatment resistance remains unclear.

The transcription factor EB (TFEB) plays a central role in the transcriptional regulation of the autophagy-lysosomal pathway (Zhang *et al*., 2025b).Under physiological conditions, mTORC1-mediated phosphorylation of TFEB promotes its retention in the cytoplasm. When mTORC1 activity is inhibited, TFEB is dephosphorylated and translocates to the nucleus, where it initiates transcription of autophagy-related genes (Akayama *et al*., 2025; Dias *et al*., 2025). However, whether TFEB directly regulates the transcription of ER-phagy-specific receptors to drive ER-phagy activation under ERS conditions has not been reported in TNBC.More importantly, the functional outcome of this regulatory axis, if abnormally activated, remains unclear: does it promote cell adaptation or trigger cell death?

Everolimus, a classic mTORC1 inhibitor, has shown clinical efficacy in renal cell carcinoma and some neuroendocrine tumors. However, single-agent everolimus has shown very limited efficacy in breast cancer, with an objective response rate of only 4.17% and a median progression-free survival of only 1.87 months in advanced TNBC (Fan *et al*., 2024).Even in relatively well-treated hormone receptor-positive breast cancer, the median progression-free survival is only 4.6 to 5.1 months (Patel *et al*., 2025).This limited efficacy suggests that TNBC cells may possess specific adaptive resistance mechanisms to everolimus. In this study, we hypothesized that everolimus inhibits mTORC1, thereby relieving mTORC1-mediated TFEB phosphorylation, promoting TFEB nuclear translocation and transcriptional upregulation of ER-phagy receptors and ultimately overactivating ER-phagy. In TNBC cells already burdened by high ERS, this overactivated ER-phagy may exceed the threshold of protective autophagy, shifting from an adaptive mechanism to a lethal event and ultimately causing TNBC cell death.

To test this hypothesis, we used two TNBC cell lines, MDA-MB-231 and MDA-MB-468 and combined immunofluorescence, nucleocytoplasmic fractionation followed by Western blotting, ChIP-qPCR, an mCherry-GFP-KDEL reporter assay, transmission electron microscopy, siRNA knockdown and complementation experiments.To investigate whether everolimus promotes TFEB nuclear translocation by inhibiting mTORC1, whether nuclear TFEB directly upregulates the transcription of ER-phagy receptors FAM134B, RTN3L and CALCOCO1 and whether over-activation of ER-phagy mediates the anti-TNBC effect of everolimus. This research also examined whether FAM134B is a key effector in this pathway. This study aimed to clarify the role of TFEB-mediated ER-phagy in everolimus-treated TNBC models and to provide an experimental basis for optimizing TNBC treatment strategies and identifying potential predictive biomarkers of efficacy.

MATERIALS AND METHODS

Cell lines

The human TNBC cell lines MDA-MB-231 (RRID: CVCL_0062; stromal-like/basal B subtype; ATCC catalog number HTB-26) and MDA-MB-468 (RRID: CVCL_0419; basal-like/basal A subtype; ATCC catalog number HTB-132) were purchased from ATCC (Manassas, VA, USA). MDA-MB-231 cells were used at passages 5–15 and MDA-MB-468 cells were used at passages 4–14. The two cell lines represent two major TNBC subtypes with markedly different biological behaviors and treatment responses: MDA-MB-231 is highly invasive and chemoresistant, whereas MDA-MB-468 represents another basal-like subtype. Using both cell lines helps preliminarily assess the generality of our findings. Cells were cultured in high-glucose DMEM (11965092, Gibco) supplemented with 10% fetal bovine serum (10099141, Gibco) and 1% penicillin/streptomycin (15140122, Gibco). Cells were maintained in a humidified incubator (model 3111, Thermo Fisher Scientific, Waltham, MA, USA) at 37 °C with 5% CO2 and saturated humidity. All cell lines were authenticated by STR profiling (Fig. S1 and Table S1) and routinely tested for mycoplasma contamination using the MycoAlert kit (Lonza, Basel, Switzerland); all results were negative.

Drugs and treatments

Everolimus (S1120, Selleck Chemicals, Houston, TX, USA) was dissolved in dimethyl sulfoxide (DMSO; D2650, Sigma-Aldrich) to prepare a 10 mM stock solution, which was aliquoted and stored at -20ºC. For experiments, the stock solution was diluted in complete medium to final concentrations of 0.1, 1, 10, 50 and 100 nM. The final DMSO concentration was kept below 0.001% (v/v) in all groups, including the vehicle control, which contained the same DMSO concentration as the treatment groups. A concentration of 50 nM was selected for mechanistic studies because it approximated the IC50 values of both cell lines at 48–72 h (see Results 3.1), produced robust mTORC1 inhibition and TFEB nuclear translocation in preliminary experiments and falls within the clinically achievable plasma trough concentration range (approximately 20–80 nM) reported for everolimus at standard dosing (10 mg/day).For autophagic flux blocking experiments, chloroquine (C6628, Sigma-Aldrich; final concentration 20 μM) or bafilomycin A1 (B1793, Sigma-Aldrich; final concentration 100 nM) was added 1 h before the end of everolimus treatment.

Cell viability assay (CCK-8)

Cells were seeded at 5 × 10^3 cells/well in 96-well plates (3599, Corning, NY, USA) and cultured overnight before treatment with 0, 0.1, 1, 10, 50, or 100 nM everolimus for 24, 48, or 72 h. Each concentration-time combination was tested in six replicate wells and each experiment was repeated three times independently (three biological

Article in Press

replicates). At the end of treatment, 10 μL of CCK-8 solution (Cell Counting Kit-8; CK04, Dojindo, Kumamoto, Japan) was added to each well and the plates were incubated at 37°C for 2 h. The absorbance at 450 nm was measured using a microplate reader (Synergy H1, BioTek Instruments, Winooski, VT, USA). Cell viability was expressed as the percentage of absorbance in the treatment group relative to the vehicle control group (0 nM, containing the same amount of DMSO) GraphPad Prism 9.0 was used to fit the concentration-response curve (four-parameter logistic equation) and calculate the IC_{50}. IC_{50} values are expressed as mean ±SD.

Apoptosis detection (Flow Cytometry)

Cells were seeded at 2×10^5 cells/well in 6-well plates. After treatment with 50 nM everolimus for 48 h, cells were collected by digestion with 0.25% EDTA-free trypsin (25200056, Gibco). Staining was performed using an Annexin V-FITC/PI apoptosis detection kit (V13241, Invitrogen, Carlsbad, CA, USA). Flow cytometry was performed on a FACS Canto II flow cytometer (BD Biosciences, Franklin Lakes, NJ, USA) and 10,000 events were acquired per sample. Data were analyzed using FlowJo software (v10.8, BD Biosciences, Franklin Lakes, NJ, USA). The gating strategy was as follows: first, an FSC-A/SSC-A scatter plot was used to define the main cell population and exclude debris; then, an FSC-A/FSC-H scatter plot was used to exclude doublets. Fluorescence compensation for Annexin V-FITC and PI was adjusted using single-stained controls. Annexin V-FITC single-positive cells were considered early apoptotic cells, Annexin V-FITC/PI double-positive cells were considered late apoptotic cells and the total apoptosis rate was the sum of the two.

Immunofluorescence staining (TFEB nuclear translocation)

Cells (2×10^4/ well) were seeded on Nunc™ Lab-Tek™ 8-well chamber glass slides. After treatment with 50 nM everolimus for 0, 5, 30, or 120 min, cells were fixed with 4% paraformaldehyde (158127, Sigma-Aldrich) for 15 min at room temperature and permeabilized with 0.1% Triton X-100 (T8787, Sigma) for 10 min. Cells were then blocked with 5% BSA (A7906, Sigma) for 1 h at room temperature, incubated with primary antibody (anti-TFEB; A303-673A, Bethyl; 1:500) overnight at 4°C and then incubated with Alexa Fluor 488-labeled secondary antibody (A11008, Invitrogen; 1:400) for 1 h at room temperature. Nuclei were counterstained with DAPI (catalog number D1306, Invitrogen, final concentration 1μg/mL) for 5 min. Representative images were acquired with a confocal microscope (TCS SP8, Leica Microsystems, Wetzlar, Germany) using a 63× oil-immersion objective and quantified in ImageJ software (v1.53, National Institutes of Health, Bethesda, MD, USA). Five fields were randomly selected from each chamber slide and ImageJ software (v1.53, NIH) was used to calculate the percentage of cells with higher TFEB fluorescence intensity in the nucleus than in the cytoplasm among at least 200 cells. All image acquisition and quantitative analyses were performed under blinded conditions by two independent researchers and mean values were used for statistical analysis.

Nucleocytoplasmic separation and Western blotting

Cytosolic and nuclear fractions were collected separately using the NE-PER Nuclear and Cytoplasmic Extraction Kit (78833, Thermo Fisher Scientific, Waltham, MA, USA) according to the manufacturer's instructions. Protein concentration was determined using the BCA method (23225, Thermo Fisher Scientific, Waltham, MA, USA). Thirty micrograms of total protein were loaded, separated by electrophoresis on a 10% or 12% SDS-polyacrylamide gel and transferred to a PVDF membrane (IPVH00010, Millipore, Burlington, MA, USA) by wet transfer. Membranes were blocked with 5% skim milk for 1 h at room temperature and then incubated with primary antibodies overnight at 4 °C. The antibodies used were as follows: The antibodies used were as follows: rabbit anti-phospho-S6K (Thr389) (9234, CST; 1:1000), rabbit anti-S6K (9202, CST; 1:1000), rabbit anti-p-4E-BP1 (Thr37/46) (2855, CST, 1:1000), rabbit anti-4E-BP1 (9644, CST, 1:1000), rabbit anti-TFEB (A303-673A, Bethyl, 1:2000), rabbit anti-LC3B (2775, CST, 1:1000), mouse anti-p62 (88588, CST, 1:2000), rabbit anti-FAM134B (PA5-52632, Invitrogen, 1:500), rabbit anti-RTN3L (ab237720, Abcam, 1:500), rabbit anti-CALCOCO1 (HPA045085, Sigma-Aldrich, 1:500), rabbit anti-IRE1α (3294, CST, 1:1000), rabbit anti-CHOP (2895, CST, 1:1000), rabbit anti-p-eIF2α (Ser51) (9721, CST, 1:1000), mouse anti-GAPDH (60004-1-Ig, Proteintech, 1:500, cytoplasmic control) and rabbit anti-lamin B1 (13435, CST, 1:1000, nuclear control). After washing, membranes were incubated with HRP-labeled secondary antibodies for 1 h at room temperature, developed with ECL chemiluminescence substrate (WBKLS0500, Millipore, Burlington, MA, USA) and quantified by gray value using ImageJ software (v1.53, National Institutes of Health, Bethesda, MD, USA). Relative expression of the target protein was calculated as the ratio of the target protein gray value to that of the internal reference protein, with the control group normalized to 1. All Western blotting experiments were repeated three times independently, each time using independently prepared protein samples.

Chromatin immunoprecipitation (ChIP)

Cells in 10-cm dishes (5×10^6/ dish) were treated with 50 nM everolimus for 2 h. ChIP experiments were then performed using the EpiQuik™ ChIP kit (P-2002, Epigentek, Farmingdale, NY, USA)according to the manufacturer's instructions. Each sample was immunoprecipitated with 2 μg of anti-TFEB antibody (A303-673A, Bethyl) or 2 μg of rabbit IgG isotype control (2729S, CST). Samples without antibody were

Article in Press

used as input controls. Specific primers were designed to amplify the CLEAR elements (E-box-like sequence: GTCACGTGAC) in the promoters of FAM134B. Meanwhile, the -2000 to -1800 bp region upstream of each gene's transcription start site was used as a non-CLEAR negative control. All ChIP-qPCR reactions were set up in three technical replicates and the results were first normalized to the input Ct value (relative enrichment = 2^(Ct_input-Ct_IP) × 100%) and expressed as input percentage. ChIP-qPCR was performed on a QuantStudio 5 Real-Time PCR System (Applied Biosystems, Foster City, CA, USA).

To verify the dependence of TFEB nuclear translocation and promoter binding on mTORC1 signaling, TSC2 knockout mouse embryonic fibroblasts (TSC2-/- MEFs) and their wild-type controls (TSC2+/+).These cells were kindly provided by Dr. David J. Kwiatkowski (Brigham and Women's Hospital, Harvard Medical School, Boston, MA, USA) and were routinely cultured in DMEM high-glucose medium. The absence of TSC2 protein in TSC2-/- cells was confirmed by Western blotting, which resulted in constitutively activated mTORC1 (as verified by elevated p-S6K levels even under basal conditions). These TSC2-/- cells were treated with everolimus (50 nM, 2 h) or vehicle, followed by ChIP-qPCR analysis of TFEB binding to the CLEAR elements of FAM134B, RTN3L and CALCOCO1 promoters. The loss of TFEB binding in TSC2-/- cells, where mTORC1 cannot be suppressed by everolimus, served to confirm that the observed TFEB–promoter interaction is dependent on mTORC1 inhibition.

Small interfering RNA (siRNA) transfection

SiRNAs targeting TFEB, FAM134B, RTN3L and CALCOCO1 and negative controls, were purchased from Dharmacon (Horizon Discovery, Lafayette, Colorado, USA). The siRNA sequences are detailed in tables 1 and 2. Based on the knockdown efficiency screening results from the pre-experiment (Fig. S2), siTFEB#1 was selected for subsequent experiments (knockdown efficiency was >70%, the most efficient of the two candidate siRNAs). Cells were seeded in 6-well plates at the appropriate density and, after 24 h of culture (approximately 50-60% confluence), were transfected with Lipofectamine RNAiMAX (13778150, Invitrogen, Carlsbad, CA, USA) according to the product instructions. The final siRNA concentration was 50 nM (this concentration showed optimal knockdown efficiency and no significant cytotoxicity in the pilot experiment; data not shown). 48 hours after transfection, some cells were collected to assess knockdown efficiency by Western blotting (the percentage decrease in protein expression was calculated relative to untransfected cells). The remaining cells were used directly for subsequent drug intervention experiments. To ensure the reliability of the experiment, parallel verification wells to assess transfection efficiency were included in each independent experiment and only batches with knockdown efficiency >70% were used in subsequent functional experiments.

Endoplasmic reticulum autophagy reporter assay (mCherry-GFP-KDEL)

First, the pLVX-mCherry-GFP-KDEL lentiviral vector (Clontech, Mountain View, CA, USA) was constructed. The sequence encoding the ER retention signal KDEL (5'-AAGGACGAGCTG-3') was inserted into the pLVX-Puro vector (Clontech, Mountain View, CA, USA) together with the mCherry-GFP fusion gene (constructed in the Laboratory of Nanjing First Hospital, Nanjing Medical University and validated by sequencing). Viral particles were packaged in HEK293T cells using a third-generation lentiviral packaging system (psPAX2 and pMD2.G; Addgene, Watertown, MA, USA). MDA-MB-231 cells were infected with the virus and stable cell lines were selected with puromycin (2 μg/mL; A1113803, Gibco, Waltham, MA, USA). After 48 h of everolimus treatment, mCherry and GFP fluorescence intensities were measured using a FACS Canto II flow cytometer (BD Biosciences, Franklin Lakes, NJ, USA) and the median mCherry/GFP fluorescence intensity ratio was calculated. Ten thousand live cell events were acquired for each experiment and the experiments were independently repeated three times.

Transmission electron microscopy

After 48 h of treatment, cells were washed with PBS, then 2.5% glutaraldehyde (Electron Microscopy grade; 16020, Electron Microscopy Sciences, Hatfield, PA, USA) was added, fixed at room temperature for 30 min and then transferred to 4 °C for fixation overnight. The next day, cells were postfixed with 1% osmium tetroxide (19100, Electron Microscopy Sciences, Hatfield, PA, USA) for 1 h, dehydrated through a graded ethanol series (50%, 70%, 90% and 100%), treated with propylene oxide and embedded in Epon 812 resin (14120, Electron Microscopy Sciences, Hatfield, PA, USA). Sections about 70 nm thick were cut using an ultramicrotome (Leica EM UC7, Leica Microsystems, Wetzlar, Germany), stained with 2% uranyl acetate and lead citrate (Electron Microscopy Sciences, Hatfield, PA, USA) and then viewed in an HT7800 transmission electron microscope (Hitachi High-Tech, Tokyo, Japan) at an acceleration voltage of 80 kV. Twenty images (5,000× and 20,000× magnification) were randomly collected for each sample. Er autophagosomes were counted independently by two pathology professionals who were not involved in the trial-group assignments and were unaware of (blinded) the trial assignments. An autophagosome is defined as a structure formed by endoplasmic reticulum (ER) debris or swollen ER encapsulated by a bilayer membrane structure. The proportion of swollen ER cells was also recorded. The counts of the two observers were averaged for statistical analysis. The inter-observer agreement was

Article in Press

Table 1: Primer sequences.

Target gene promoter	Primer direction	Primer sequence (5′→3′)
FAM134B	Forward	TCCCAGAGCTCTTCGGAGTT
	Reverse	AGCTGTGCCTCTGGTTTGAG
RTN3L	Forward	ATCGTTGCAGCTGAGGTAGG
	Reverse	GCCGCAGAGTTTCCTAGTCA
CALCOCO1	Forward	GCACCTGAGAACTAGCGCTA
	Reverse	GTCCGGAGGAACTGGATAGA

Table 2: Sequence information.

siRNA	Gene	Sequence direction	Sequence (5′→3′)
siTFEB#1	TFEB	Sensitive strand	GAAGGUGCUACAGAAGUUU
siTFEB#2	TFEB	Sensitive strand	CAAAGAUCCUCGAGAUUA
siFAM134B	FAM134B	Sensitive strand	GGCAUGGAGCUGUUCAUAA
siRTN3L	RTN3L	Sensitive strand	GCAGUGUUUGCUGGACUUA
siCALCOCO1	CALCOCO1	Sensitive strand	GGAUCGGCUCAUCAGAUUU
siNC	Negative control (non-targeted)	Sensitive strand	UUCUCCGAACGUGUCACGU

evaluated by calculating the intraclass correlation coefficient (ICC) (ICC>0.85 was considered as good agreement).

Animal experiments

Ethical statement

The animal experimental protocol was approved by the institution's animal committee (IACUC-2024-0157) and all procedures were conducted in accordance with the NIH Guidelines for the Care and Use of Laboratory Animals. All animal experiments were reported in accordance with ARRIVE guidelines.

Xenograft tumor model

Female BALB/c nude mice (4-5 weeks old, weighing 18-20 g; Beijing Weitong Lihua Laboratory Animal Technology Co., Ltd., Beijing, China) were maintained in an SPF animal room (Mice were maintained in the SPF animal facility of Nanjing First Hospital, Nanjing Medical University, at 22 ± 2 °C, 50 ± 10% humidity, with a 12-h light–dark cycle and food and water ad libitum). MDA-MB-231 cells (5×10^6 cells, suspended in 100 μL of a 1:1 mixture of serum-free DMEM and Matrigel (354234, Corning, Corning, NY, USA)) were subcutaneously injected into the right axillary area.When the tumor volume reached approximately 100 mm^3 (about 7 days after inoculation), mice were ranked by tumor volume and allocated alternately to the two groups (n = 8 each) using a stratified randomization method based on tumor size at baseline: (1) Vehicle control group: equal amounts of vehicle (5% DMSO, 30% PEG300 and 65% saline) were orally administered daily; (2) Everolimus group: everolimus 5 mg/kg (dissolved in the above vehicle) was given orally daily. The dose selection was based on the following criteria: (a) 5 mg/kg/ day showed significant anti-tumor effect and was well tolerated in the pilot study; (b) This dose is equivalent to a human clinical dose of approximately 10 mg/d based on body surface area. Tumor measurements were performed in a blinded manner: the long (a) and short (b) diameters of the tumor were measured every 3 days by an investigator who was not involved in the grouping of animals and was unaware of it, using an electronic vernier caliper and the tumor volume was calculated as $a \times b^2 / 2$. At the same time, mice were weighed every 3 days and the curve of body weight change over time was recorded to dynamically evaluate drug tolerance, rather than relying only on the end-point initial body weight difference. After 21 days of continuous administration, animals were euthanized by CO_2 inhalation (using a CO_2 euthanasia chamber, model 101, VetEquip, Pleasanton, CA, USA) and tumor tissues were isolated and weighed. One portion of the tumor tissue was fixed in 4% paraformaldehyde for immunohistochemistry and the other portion was immediately snap-frozen in liquid nitrogen and stored at −80°C for protein extraction. The sample size estimation was based on the pre-experimental effect size (expected tumor volume reduction of 50%), set α=0.05, β=0.2 (power of 80%) and indicated that at least 7 mice per group were needed. Given the possible exclusion, 8 mice per group were included. Tumor tissue photographs only show the endpoint tumors dissected after sacrifice (21 days of intervention).

Immunohistochemistry

Paraffin-embedded tissue sections (4 μm thick) were successively deparaffinized and hydrated and antigen retrieval was performed with sodium citrate buffer (pH 6.0) at 95ºC for 20 min (using a water bath, model WB-10, Major Science, Saratoga, CA, USA). Sections were incubated in 3% hydrogen peroxide solution for 10 min to inactivate endogenous peroxidase. The cells were then blocked with 5% normal goat serum at room temperature for 1 h, followed by incubation with primary antibodies at 4°C overnight: rabbit anti-Ki-67 (catalogue number 12202, CST, 1:200), rabbit anti-TFEB (A303-673A,

Article in Press

Bethyl, 1:200), rabbit anti-LC3B (2775, CST, 1:200). After washing with PBS, the cells were incubated with HRP-labeled goat anti-rabbit secondary antibody (catalog number 7074, CST, 1:500) for 1 h at room temperature. DAB chromogenesis solution (ZLI-9018, ZSGB-BIO) was used for color development and the slides were counterstained with hematoxylin. Images were acquired using a Pannoramic MIDI digital slide scanner (3DHistech, Budapest, Hungary). All immunohistochemical scores were performed under blinded conditions: scores were determined independently by two pathology professionals unaware of the trial-group assignments. Ki-67 positivity was assessed: five high-power fields (400x) were randomly selected from the tumor area of each section and at least 500 cells were counted in each field to determine the percentage of positive cells. TFEB nuclear positivity: clear brown particles in the nucleus were defined as positive and the proportion of nuclear-positive cells was calculated. LC3B expression: cells with punctate or circular cytoplasmic staining were counted as positive and the proportion of positive cells was calculated. The scores of the two observers were averaged and if there was any disagreement (difference >10%), the two observers would reevaluate together to reach a consensus.

Tumor tissue protein extraction and western blot

Approximately 50 mg of frozen tumor samples were weighed and placed in RIPA lysis buffer (R0278, Sigma-Aldrich, St. Louis, MO, USA) containing protease inhibitors (cOmplete Mini, Roche, Basel, Switzerland) and phosphatase inhibitors (PhosSTOP, Roche, Basel, Switzerland). The tissue was homogenized using a TissueLyser II (Qiagen, Hilden, Germany) at 30 Hz for 2 min. The homogenate was centrifuged at 12,000 ×g for 15 min at 4°C and the supernatant was collected. Centrifugation was performed using a refrigerated centrifuge (model 5424R, Eppendorf, Hamburg, Germany). Protein concentrations were quantified using the BCA assay. The procedure for Western blotting was the same as that of the cell experiment (Section 2.6). Four mice (n=4) were used in each group for tumor tissue Western blotting, while 6 mice (n=6) were used in each group for immunohistochemistry. The reasons for the difference in sample size between the two groups were as follows: the amount of tissue required for Western blotting was large and some tumor tissues were allocated to immunohistochemistry and RNA extraction experiments first, resulting in fewer samples available for Western blotting. For immunohistochemistry, 6 animals were randomly selected from each group for staining and scoring. The sample sizes of both experiments met the requirements for statistical analysis. The mouse source used in the Western blot and IHC experiments was the same batch of animals and all animal numbers and grouping information were recorded.

Statistical analysis

Data are presented as mean ± standard deviation (SD) and statistical analysis was performed using GraphPad Prism 9.0 (GraphPad Software, San Diego, CA, USA). A two-tailed Student's t test (normally distributed data) or a Mann-Whitney U test (non-normally distributed data) was used to compare the two groups. A one-way ANOVA was used to compare multiple groups, followed by a Tukey HSD post hoc test. Experiments involving two factors, time and treatment, were performed using two-way ANOVA followed by Sidak's post hoc multiple comparison test. Before ANOVA analysis, the Shapiro-Wilk test was used to evaluate the normality of the data ($P>0.05$ was considered to meet the normality requirement) and the Levene test was used to evaluate the homogeneity of variance ($P>0.05$ was considered to meet the homogeneity of variance), both of which met the prerequisites for analysis. If not, the corresponding nonparametric test (Kruskal-Wallis test) was used. All statistical tests were two-tailed and results were reported with effect sizes (Cohen's d or η^2) and 95% confidence intervals (CIs) to enhance interpretability. Tukey or Sidak correction was used for multiple comparisons to control the type I error rate. The sample size estimate was based on the effect size from the pilot study ($\alpha=0.05$, $\beta=0.2$, power=80%). The Grubbs test was used to identify and eliminate outliers ($\alpha=0.05$). A total of two data points (one from the CCK-8 pre-experiment and one from the electron microscope counting experiment) were excluded. All *in-vitro* experiments were independently repeated 3 times (i.e., 3 biological replicates) and technical Wells were set up in each replicate. *In-vivo* immunohistochemistry was performed in 6 mice per group and Western blotting in 4 mice per group. A P value of less than 0.05 was considered to indicate statistical significance.

RESULTS

Everolimus inhibits TNBC cell proliferation and induces cell death

CCK-8 assay showed that everolimus inhibited the viability of MDA-MB-231 and MDA-MB-468 cells in a concentration - and time-dependent manner (Fig. 1A). The cell viability of both cell lines was significantly decreased in the everolimus treatment group at 10 nM and higher concentrations, while there was no significant difference between the 1 nM treatment group and the control group ($P>0.05$). The calculated IC_{50} values for MDA-MB-231 cells were 78.6+6.2 nM (24 h), 52.3+4.8 nM (48 h) and 38.7+3.5 nM (72 h); for MDA-MB-468 cells, the IC_{50} values were 92.4+7.1 nM (24 h), 58.6+5.3 nM (48 h) and 42.1+4.0 nM (72 h). The complete concentration-activity curves of the two cell lines at three time points of 24, 48 and 72 hours are presented in figure 1A, where the inhibition rate of MDA-MB-231 cells was 77.55% after treatment with 50 nM everolimus for 72 hours. Flow cytometry results showed that the total

Article in Press

apoptosis rate (Annexin V-positive cells) significantly increased from 6.2% in the control group to 34.7% after 48 hours of treatment with 50 nM everolimus (Fig. 1B; early, late and total apoptosis rates are shown in bars, respectively, with total apoptosis rate presented separately). The number of ER autophagosomes (0.34+0.09 vs. 5.68+1.02, $P < 0.001$) was significantly higher in the everolimus-treated group than in the control group. The number of ER autophagosomes and the proportion of ER swelling cells were significantly increased in the everolimus-treated group compared with the control group (4.87% ± 1.12% vs. 78.24% ± 6.23%; Table 3; $P < 0.05$).

Everolimus inhibits mTORC1 and promotes TFEB nuclear translocation

Western blotting showed a concentration-dependent decrease in p-S6K and p-4E-BP1 levels after 2 h of everolimus treatment in the range of 1-100 nM, confirming the inhibition of mTORC1 activity (Fig. 2A). In the control group, TFEB was mainly localized in the cytoplasm. After everolimus treatment, TFEB rapidly translocated to the nucleus, with nuclear accumulation beginning at 30 minutes and peaking at 2 hours (Fig. 2B). Immunofluorescence analysis further confirmed that the proportion of TFEB nuclear-positive cells increased from 8.6% in the control group to 76.3% after 2 hours of treatment with 50 nM everolimus ($P<0.05$). The quantitative results are presented as bar charts and representative immunofluorescence images show TFEB localization at 0, 5, 30 and 2 hours (Fig. 2C).

Everolimus induces endoplasmic reticulum autophagy and upregulates specific receptor expression

Western blotting showed that everolimus increased LC3-II expression and decreased p62 levels in a concentration-dependent manner (Fig. 3A). After blocking lysosomal degradation with Baf A1, LC3-II accumulation was greater in the everolimus group, indicating enhanced autophagic flow (Figs. 3B-3E). Importantly, protein levels of the endoplasmic reticulum autophagy receptors FAM134B, RTN3L and CALCOCO1 were significantly increased after everolimus treatment, peaking at 48 hours (Fig. 3C), which increased to 4.32-fold, 3.18-fold and 2.76-fold, respectively, as compared with the control group ($P<0.05$). The mCherry-GFP-KDEL reporter gene assay showed that the mCherry/GFP ratio in the everolimus-treated group (0.81+0.09) was significantly higher than that in the control group (0.23+0.04) ($P<0.001$) (Fig. 3D).

TFEB is essential for everolimus-induced endoplasmic reticulum autophagy

To verify the key role of TFEB, TFEB was knocked down using siRNA. Figures 4A and 4B show the knockdown efficiency verification results of siTFEB#1 and siTFEB#2, respectively, where siTFEB#1 was selected for subsequent experiments with a knockdown efficiency of about 82%. Everolimus-induced upregulation of FAM134B, RTN3L and CALCOCO1 was significantly blocked by knockdown of TFEB (Fig. 4C). In addition, the previously elevated LC3-II and reduced p62 levels were partially reversed ($P<0.05$) (Fig. 4D). ChIP-qPCR showed that everolimus enhanced the binding of TFEB to CLEAR elements in the promoter regions of FAM134B, RTN3L and CALCOCO1 (expressed as Input%, with no significant enrichment in IgG control and no TFEB binding signal in the negative control region). However, this binding was lost in $TSC2^{-/-}$ cells (constitutively activated mTORC1) (Fig. 4E). These results demonstrate that, in the everolimus-treated TNBC model, TFEB directly binds to and transcriptionally upregulates ER-phagy receptor genes in an mTORC1-dependent manner. Functionally, knockdown of TFEB partially attenuated the inhibitory effect of everolimus on cell proliferation (Table 4): under siNC condition, everolimus reduced cell viability to 55.23%, 36.77% and 22.45% at 24, 48 and 72 hours, respectively; however, under siTFEB condition, the cell viability was still maintained at 78.92% for 72 hours, indicating that TFEB knockdown partially reversed the everolimus-induced inhibition of cell viability. Two-way analysis of variance showed that the drug-time interaction was significant ($F = 12.9$, $P < 0.01$). Knockdown of TFEB also significantly reduced everolimus-induced ER disruption and the number of autophagosomes (Table 5).

The endoplasmic reticulum autophagy receptor FAM134B is indispensable in the anti-TNBC effect of everolimus

As shown in figure 5A, knockdown of FAM134B (siFAM134B) significantly attenuated everolimus-induced inhibition of cell viability at all time points examined. At 72 hours, cell viability in the siFAM134B+everolimus group was 78.92%+6.23%, compared to 22.45%+3.56% in the siNC+everolimus group ($P < 0.001$) and 100.00%+4.92% in the siNC+control group. In contrast, knockdown of RTN3L resulted in 72-hour cell viability of 31.23%+4.12% ($P > 0.05$ vs. siNC+everolimus) and knockdown of CALCOCO1 resulted in 28.67%+3.98% ($P>0.05$ vs. siNC+everolimus). At 48 hours, the siFAM134B+everolimus group showed 85.36%+6.57% viability, while siRTN3L+everolimus and siCALCOCO1 +everolimus groups showed 38.92% ±4.56% and 35.78% ±4.23% viability, respectively (siNC+everolimus: 36.77% ±3.89%). At 24 hours, siFAM134B+everolimus maintained 92.18%±5.89% viability, whereas siRTN3L+everolimus and siCALCOCO1+everolimus groups showed 57.34%±5.12% and 54.89%±4.87% viability, respectively (siNC+everolimus: 55.23% +4.12%). The mCherry-GFP-KDEL reporter assay revealed that FAM134B knockdown almost completely reduced everolimus-induced ER-phagy flux (Fig. 5B). The mCherry/GFP ratio in the siFAM134B+everolimus group was 0.28+0.05, compared to 0.81+0.09 in the siNC+everolimus group ($P < 0.001$) and 0.23+0.04 in the siNC+control group.

Article in Press

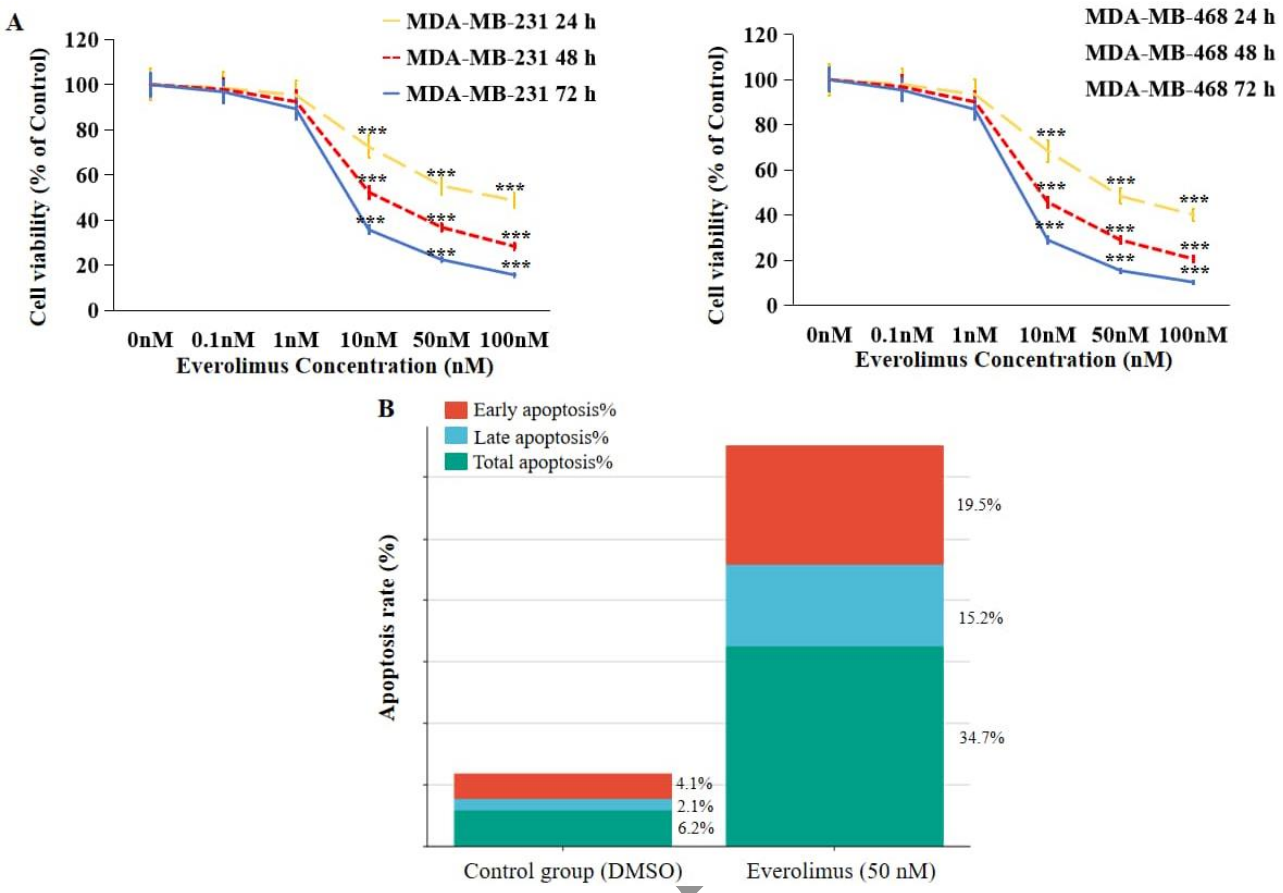

Fig. 1: Everolimus inhibits TNBC cell proliferation and induces cell death. (A) CCK-8 concentration-activity curve (MDA-MB-231 and MDA-MB-468); (B) Column chart of apoptosis rate (flow cytometry using Annexin V-FITC/PI double staining) Note: n.s., not significant; *P<0.05; **P<0.01;***P<0.001 vs. 0 nM

Table 3: Endoplasmic reticulum stress under everolimus treatment. (Transmission electron microscope, 48 hours).

Group	Number of autophagic vesicles per cell section	Percentage of swollen cells in endoplasmic reticulum	*P*
Control group	0.34±0.09	4.87±1.12	<0.001
Everolimus group (50 nM)	5.68±1.02	78.24±6.23	<0.001

Note: MDA-MB-231 cells were treated with 50 nM everolimus for 48 hours, followed by observation and counting under transmission electron microscopy. Data are expressed as mean±SD; n = 3 independent experiments, with 20 images randomly selected per experiment per group. P-values were determined using a two-tailed Student's t-test.

Knockdown of RTN3L reduced the mCherry/GFP ratio to 0.59+0.07 ($P < 0.05$ vs. siNC+everolimus) and knockdown of CALCOCO1 reduced it to 0.63+0.06 ($P < 0.05$ vs. siNC+everolimus). Both RTN3L and CALCOCO1 knockdown groups showed mCherry/GFP ratios that were significantly higher than those in the siFAM134B+everolimus group ($P < 0.01$ for both comparisons). In the rescue experiment, FAM134B was re-expressed in FAM134B-knockdown cells (Fig. 5C). At 72 hours, cell viability in the siFAM134B+FAM134B-complemented+everolimus group was 34.56%+5.12%, compared to 78.92%+6.23% in the siFAM134B +everolimus group ($P < 0.01$) and 22.45%+3.56% in the siNC+everolimus group. At 48 hours, the complemented group showed 41.23%+4.89% viability versus 85.36%+6.57% in the siFAM134B+everolimus group ($P < 0.01$) and 36.77%+3.89% in the siNC+everolimus group. At 24 hours, the complemented group showed 62.34%+5.67% viability versus 92.18%+5.89% in the siFAM134B +everolimus group ($P < 0.05$) and 55.23%+4.12% in the siNC+everolimus group. Western blotting was performed to examine the expression of key signaling molecules in FAM134B-knockdown cells (Fig. 5D).

Article

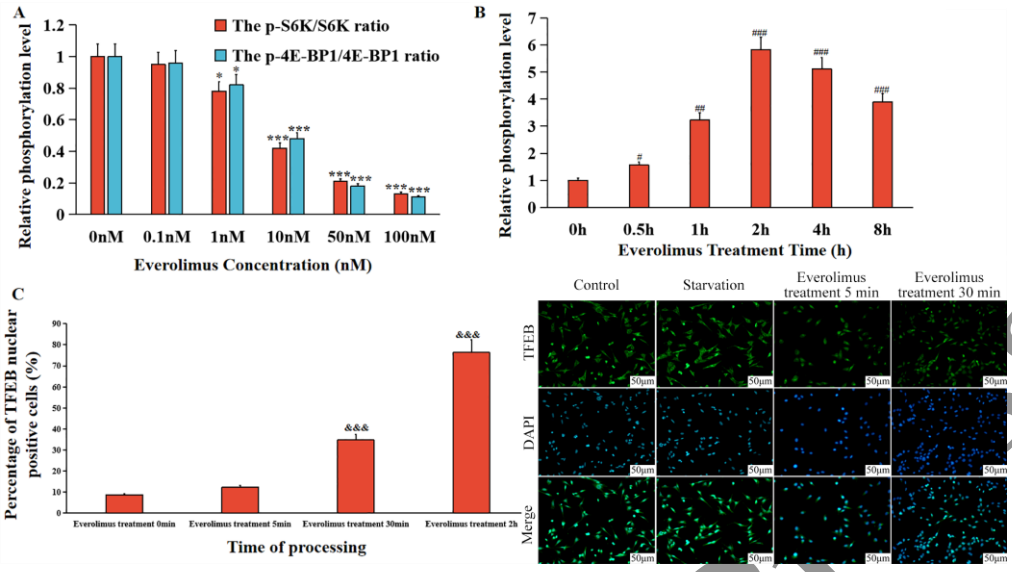

Fig. 2: Everolimus inhibits mTORC1 and promotes TFEB nuclear translocation. (A) Phosphorylation levels of downstream mTORC1 signaling proteins (quantitative bar chart based on Western blot analysis); (B) Nucleoplasmic separation of TFEB nuclear translocation (quantitative bar chart based on Western blot analysis); (C) Immunofluorescence visualization of TFEB nuclear translocation (representative image+quantitative bar chart). Note: *P<0.05;**P<0.01;***P<0.001 vs. 0 nM. #P<0.05;##P<0.01;###P<0.001 vs. 0 h. andandandP<0.001 vs. 0 minute.

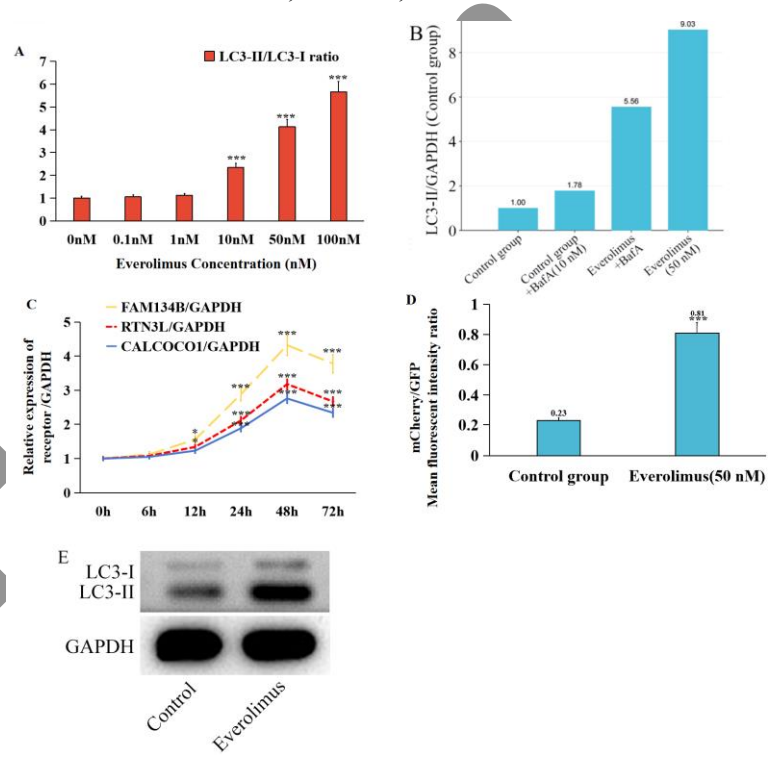

Fig. 3: Everolimus induces endoplasmic reticulum autophagy and upregulates specific receptor expression. (A) Western blot analysis of the effect of everolimus on autophagy marker expression after 24 h; (B) Baf A1 blockade assay to verify the effect of 50 nM everolimus treatment for 24 h on autophagic flux; (C) Western blot analysis of the time curve of 50 nM everolimus-induced upregulation of ER-phagy receptors; (D) Flow cytometry analysis of endoplasmic reticulum autophagy levels at 48 h using the mCherry-GFP-KDEL reporter system; (E)Baf A1 blockade assay to detect autophagic flux after 50 nM everolimus treatment.MDA-MB-231 tumor-bearing nude mice (n=5/ group) were treated with vehicle control or everolimus 2.5, 5, 10 mg/kg/d orally for 14 days. Data are presented as mean ±SEM. *P<0.05, **P<0.01, ***P<0.001 (two-way ANOVA and Sidak's post hoc multiple comparison test, compared with vehicle control group). The dose of 5 mg/kg/ day showed significant tumor suppression and was well tolerated (<5% weight loss during treatment, data not shown) and was chosen as the formal experimental dose.

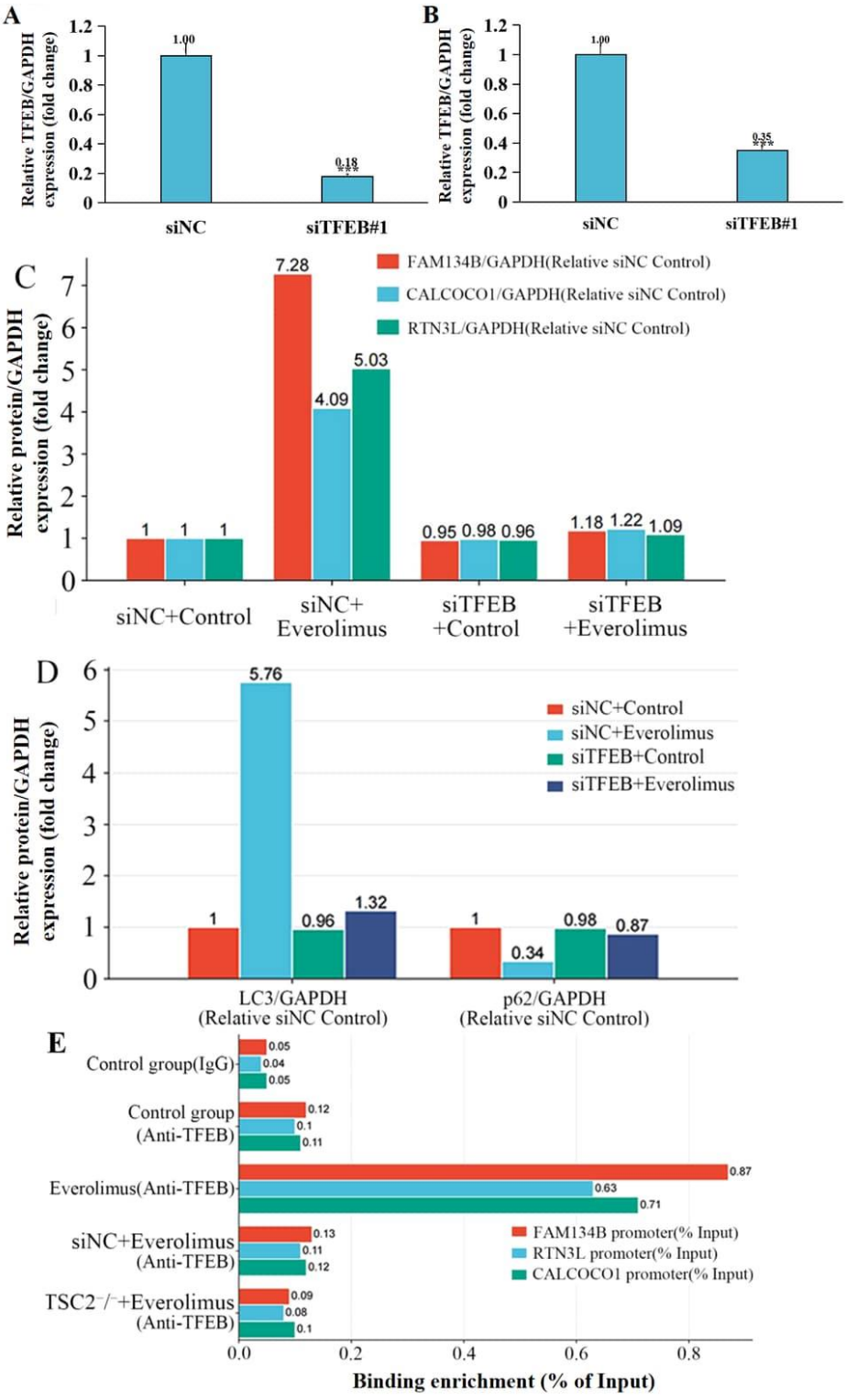

Fig. 4: TFEB is essential for everolimus-induced endoplasmic reticulum autophagy. (A) Validation of siTFEB#1 knockdown efficiency (quantitative Western blot bar chart); (B) Validation of siTFEB#2 knockdown efficiency (quantitative Western blot bar chart); (C)Blocking effect of siTFEB on the upregulation of ER-phagy receptors under 50 nM everolimus treatment by Western blot; (D) Reversal effect of siTFEB on LC3-II elevation and p62 reduction after 48 h of 50 nM everolimus treatment by Western blot; (E) Binding of TFEB to the CLEAR element of the endoplasmic reticulum autophagy receptor promoter after 2 h of 50 nM everolimus treatment by ChIP-qPCR.

Table 5: Effect of siTFEB on everolimus-induced ER-phagy formation. (Transmission electron microscopy, 50 nM everolimus, 48 h).

Group	Number of endoplasmic reticulum autophagosomes per cell section	*P* (vs. siNC+Everolimus)
siNC+Control	0.34± 0.14	<0.001
siNC+Everolimus	5.68± 1.06	-
siTFEB+ Everolimus	1.13± 0.37	<0.001

Note: Data are expressed as mean+SD, with n = 3 independent experiments; 20 images were randomly collected per experiment per group. P-values were determined using one-way ANOVA and Tukey's HSD post-hoc multiple comparison test. The effect size $\eta^2 = 0.92$.

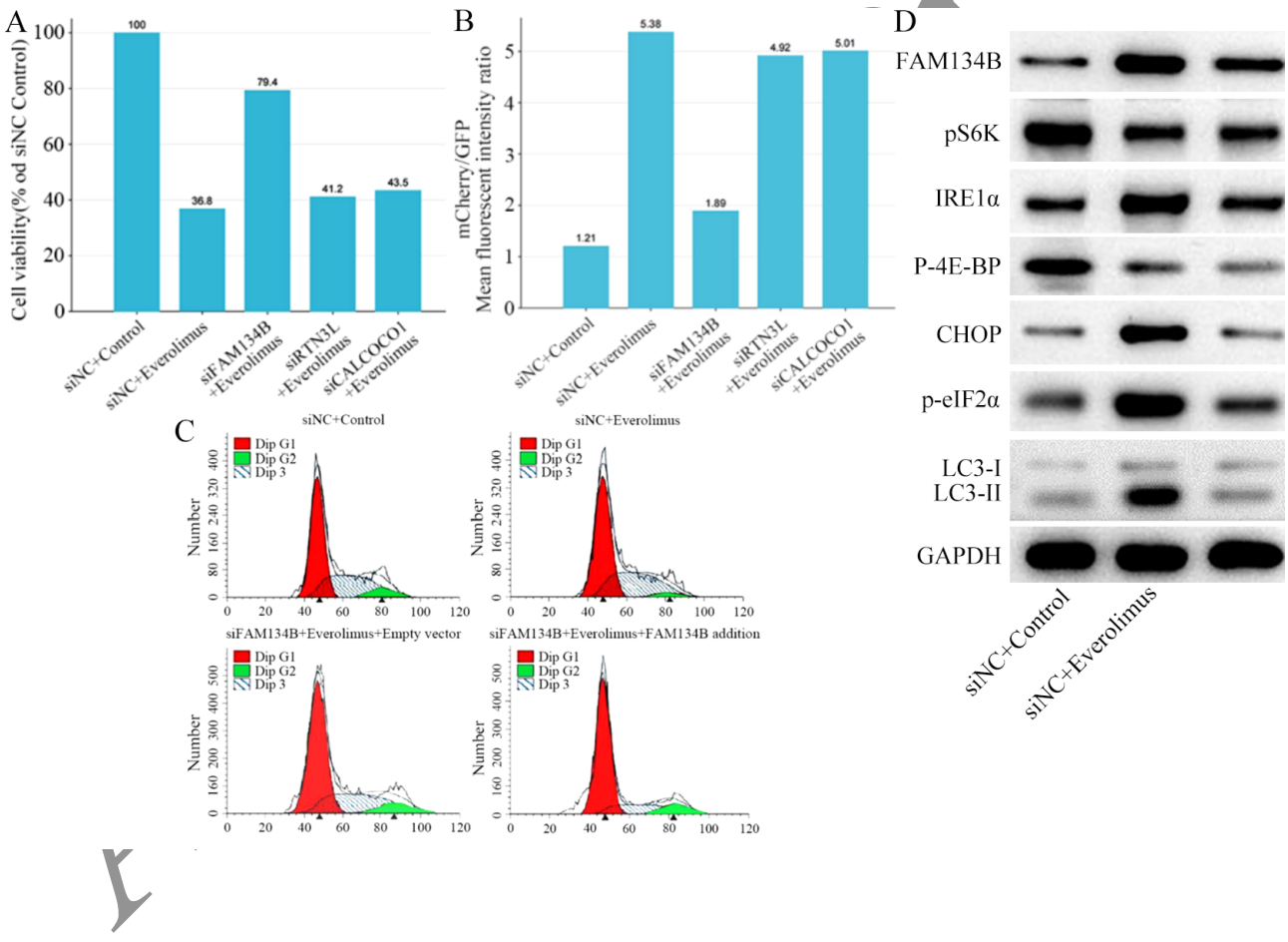

Fig. 5: The endoplasmic reticulum autophagy receptor FAM134B is indispensable in the anti-TNBC effect of everolimus. (A) CCK-8 assay to detect the effect of different ER-phagy receptor knockdowns on the cell-killing effect of 50 nM everolimus treatment for 48 h; (B) mCherry-GFP-KDEL reporter assay to detect the effect of different ER-phagy receptor knockdowns on endoplasmic reticulum autophagy induced by 50 nM everolimus treatment for 48 h; (C) FAM134B complementation assay to detect the effect of everolimus sensitivity; (D) Effect of FAM134B knockdown on everolimus-mediated protein expression.

Table 6:Effect of FAM134B knockdown on everolimus-induced morphological changes in the ER. (Transmission electron microscopy, 50 nM everolimus, 48 h).

Group	Number of ER autophagic vesicles per cell section	Proportion of swollen endoplasmic reticulum cells (%)
siNC+Control	0.34±0.12	4.68±1.60
siNC+Everolimus	5.79±1.01	77.36±6.10
siFAM134B+Everolimus	0.46±0.23	7.85±2.30

Note: Data are expressed as mean+SD, with n = 3 independent experiments; 20 images were randomly collected per experiment per group. Univariate analysis of variance and Tukey's HSD post-hoc multiple comparison test revealed that the siFAM134B+everolimus group showed a statistically significant difference compared to the siNC+everolimus group ($P < 0.001$). The effect size was $\eta^2 = 0.94$.

In siNC-transfected cells, everolimus treatment increased FAM134B expression to 4.32-fold of control, reduced p-S6K levels to 0.21+0.04 of control, reduced p-4E-BP1 levels to 0.18+0.03 of control, increased IRE1α expression to 4.56+0.42-fold of control, increased p-eIF2α to 3.89+0.35-fold of control, increased CHOP to 4.12+0.38-fold of control and increased LC3-II to 3.78+0.31-fold of control. In FAM134B-knockdown cells treated with everolimus (siFAM134B+everolimus), FAM134B expression was reduced to 0.15+0.03 of siNC+everolimus levels. p-S6K levels remained suppressed at 0.23±0.05 of control ($P > 0.05$ vs. siNC+everolimus) and p-4E-BP1 levels remained suppressed at 0.20+0.04 of control ($P > 0.05$ vs. siNC+everolimus). However, IRE1α expression was reduced to 0.67±0.09 of control, p-eIF2α to 0.72±0.08 of control, CHOP to 0.58±0.07 of control and LC3-II to 0.82±0.10 of control, all representing significant reductions compared to the siNC+everolimus group ($P < 0.001$ for all comparisons). The levels of IRE1α, p-eIF2α, CHOP and LC3-II in the siFAM134B+everolimus group were comparable to those in the siNC+control group ($P > 0.05$ for all comparisons). Transmission electron microscopy revealed that FAM134B knockdown significantly reduced everolimus-induced ER morphological abnormalities (Table 6). The number of ER autophagic vesicles per cell section in the siFAM134B +everolimus group was 0.46+0.23, compared to 5.79+1.01 in the siNC+everolimus group ($P < 0.001$) and 0.34+0.12 in the siNC+control group. The proportion of swollen ER cells in the siFAM134B+everolimus group was 7.85%+2.30%, compared to 77.36%+6.10% in the siNC+everolimus group ($P < 0.001$) and 4.68%+1.60% in the siNC+control group.

Everolimus inhibits TNBC growth and activates TFEB-mediated endoplasmic reticulum autophagy in-vivo

In the MDA-MB-231 xenograft model, continuous treatment with everolimus (5 mg/kg/day) for 21 days resulted in significant reductions in tumor volume (62.3%) and tumor weight (58.4%) compared with vehicle controls (Figs. 6A-6D). The body weight of the mice was measured every 3 days and the full body weight curves over time are presented in figure 6B, which showed no significant weight loss during treatment. Immunohistochemical staining of tumor tissue showed that the positive rate of Ki-67 in the everolimus group was significantly lower (Fig. 6C) and the percentage of TFEB nuclear-positive cells increased from 12.03%+2.77% to 58.36%+6.24% in the everolimus group. The percentage of LC3B punctate staining-positive cells increased from 8.57%+2.12% to 42.45%+4.76% (Fig. 6C). Representative immunohistochemical images are shown in figure 6E ($P<0.001$; Table 7). Western blot analysis of xenograft tumor tissues further confirmed the inhibition of p-S6K, enhanced nuclear accumulation of TFEB and up-regulation of the ER autophagy receptor FAM134B and down-regulation of p62 in the everolimus group (Fig. 6F; Table 8, n=4) ($P<0.001$).

DISCUSSION

This study systematically investigated the mechanism of action of everolimus in TNBC cells and xenograft models. The results showed that everolimus promoted TFEB dephosphorylation and nuclear translocation by inhibiting mTORC1 activity. Furthermore, nuclear TFEB directly binds to the CLEAR elements in the promoter regions of ER-phagy receptors FAM134B, RTN3L and CALCOCO1 to upregulate their expression transcriptionally and the upregulation of ER-phagy receptors drives increased ER-phagy translocation, which ultimately triggers cell death in TNBC cells. Functional screening showed that FAM134B was an indispensable downstream effector in this pathway. Together, these findings delineate the complete signaling chain of the mTORC1/TFEB/ER-phagy axis in the everolimus-treated TNBC model, providing a mechanistic explanatory framework for understanding the limited single-agent activity of everolimus in TNBC.

mTORC1 inhibition and nuclear translocation of TFEB

This study demonstrated that everolimus at 1-100 nM inhibited the phosphorylation of S6K and 4E-BP1, downstream substrates of mTORC1, accompanied by the dephosphorylation and rapid nuclear translocation of TFEB, which began to increase at 30 min after administration and peaked at 2 h. This finding is consistent with the known mTORC1-TFEB regulatory axis (Liao *et al*., 2026; Dias *et al*., 2025).

Article in Press

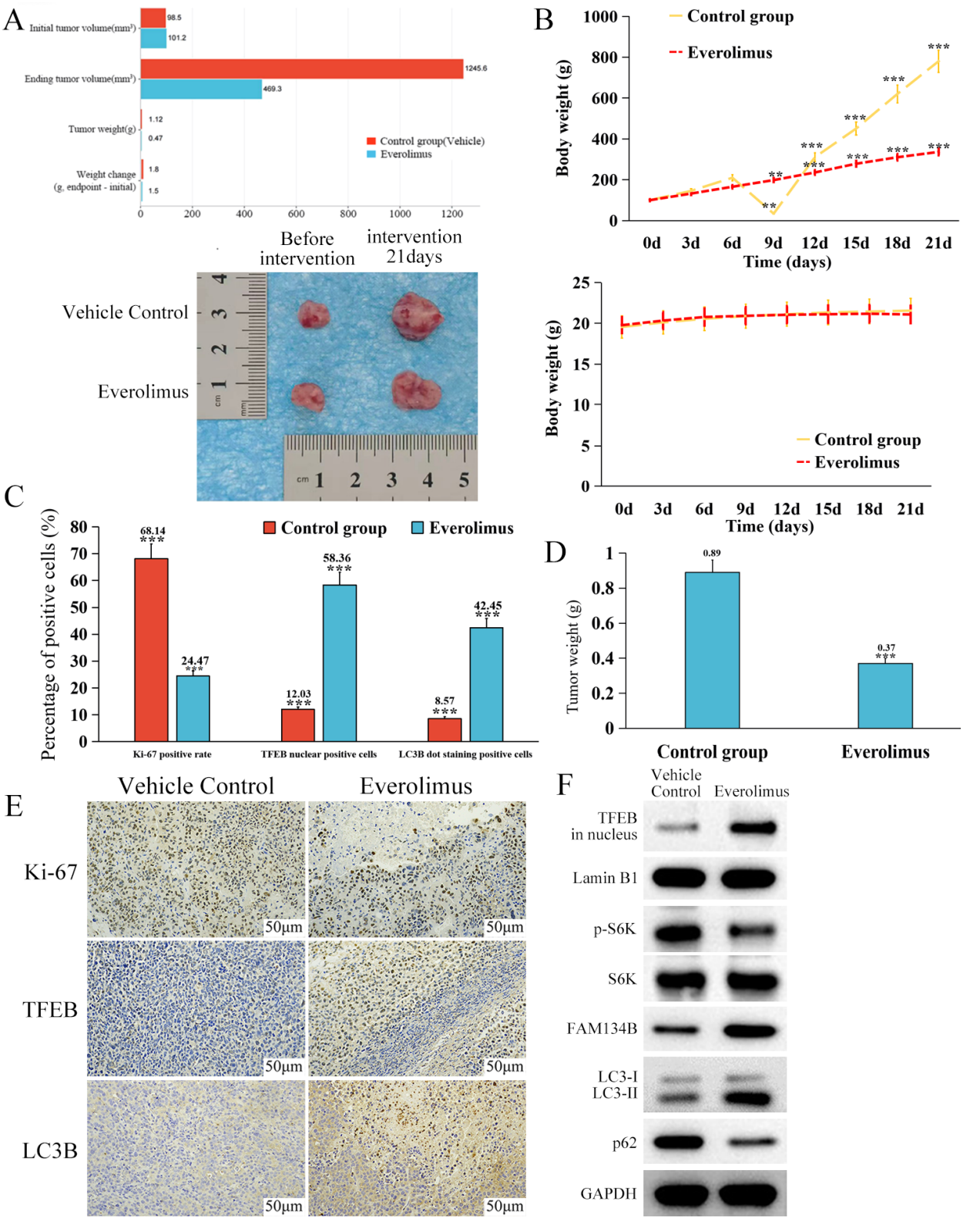

Fig. 6: Evimodine inhibits TNBC growth *in-vivo* and activates TFEB-mediated endoplasmic reticulum autophagy. (A) End-point tumor image; (B) Tumor growth curve+Weight change curve; (C) Quantitative bar chart of immunohistochemistry results; (D) Bar chart showing the weight of the terminal tumor; (E) Representative images of immunohistochemistry; (F) Representative bands from protein blotting of tumor tissue. Data are presented as mean ±SEM. *P<0.05, **P<0.01, ***P<0.001.

Table 7: LC3B punctate staining, TFEB nuclear positivity and Ki-67 positivity in xenograft tumor tissues (immunohistochemistry, n=6 per group).

Indicator	Control group	Everolimus group	t	P
Ki-67 Positive Rate (%) (n=6)	68.14±6.98	24.47±4.01	13.288	<0.001
TFEB nuclear positive cell proportion (%)	12.03±2.77	58.36±6.24	16.623	<0.001
LC3B punctate positive cell proportion (%)	8.57±2.12	42.45±4.76	15.926	<0.001

Note: Data are expressed as mean+SD. From each group, 6 mice were randomly selected for staining and scoring. Five high-magnification fields (400×) were randomly chosen from each slide, with at least 500 cells counted per field. P-values were determined using a two-tailed Student's t-test.

Table 8: Western blot validation of TFEB/ER-phagy pathway activation in xenograft tumor tissues (everolimus 5 mg/kg/day, administered continuously for 21 days, n=4 per group).

Indicators	Control group	Everolimus group	t	*P*
p-S6K/S6K (n=4)	1.00±0.09	0.24±0.06	14.052	<0.001
Intranuclear TFEB/Lamin B1 (n=4)	1.00±0.08	5.83±0.60	15.959	<0.001
FAM134B/GAPDH (n=4)	1.00±0.09	4.77±0.44	16.789	<0.001
RTN3L/GAPDH (n=4)	1.00±0.07	3.11±0.32	12.883	<0.001
CALCOCO1/GAPDH (n=4)	1.00±0.09	3.65±0.45	11.549	<0.001
LC3-II/GAPDH (n=4)	1.00±0.10	4.13±0.50	12.669	<0.001
p62/GAPDH (n=4)	1.00±0.08	0.35±0.07	12.229	<0.001

Note: Data are expressed as mean±SD. Each protein blot experiment utilized four mice per group (n=4); the smaller sample size is attributed to the substantial tissue volume required for protein blotting, but n=4 meets statistical analysis requirements. The relative expression level of target proteins was calculated as the ratio of the target protein's grayscale value to that of the internal reference protein, with the control group normalized to 1. P-values were obtained using a two-tailed Student's t-test.

Previous studies have reported that everolimus combined with melatonin can synergistically inhibit mTOR signaling and induce apoptosis (Demirkesen *et al*., 2025), consistent with this study's finding that everolimus alone can effectively block mTORC1. However, relevant clinical studies have shown that the objective response rate of everolimus (10 mg/d) monotherapy in advanced TNBC is only 4.17% and the median PFS is 1.87 months (Mehlich *et al*., 2022). This discrepancy between *in-vitro sensitivity and clinical inefficacy suggests that TNBC cells may have multiple compensatory mechanisms in the In-vivo* microenvironment that partially counterbalance the direct effects of mTORC1 inhibition.

Transcriptional regulation of ER-phagy receptors by TFEB

The key finding of this study is that TFEB nuclear translocation does not universally activate all autophagy-related genes. Still, it differentially upregulates the expression of ER-phagy-specific receptors FAM134B, RTN3L and CALCOCO1. ChIP-qPCR directly demonstrated the enhanced binding of TFEB to CLEAR elements in the promoter regions of the above receptor genes. In the context of everolimus-treated TNBC cells, these data demonstrate that TFEB acts as a transcriptional regulator of selective ER-phagy receptors, extending its known function from a "global autophagy regulator" to a more specialized role in ER-phagy regulation. Previous studies have shown that TFEB acts as a master transcription factor in the autophagy-lysosomal pathway and initiates the transcription of multiple autophagy-related genes (Wang *et al*., 2025b; Negoita *et al*., 2026). However, whether TFEB specifically regulates ER-phagy receptors and the pathophysiological significance of this regulation in the context of ER stress are not known. The present study provides experimental evidence in TNBC models that selective upregulation of ER-phagy receptors via TFEB nuclear translocation in TNBC cells with high ERS load may have important functional consequences for the everolimus response.

Activation of ER-phagy and cell fate

The functional direction of ER-phagy in TNBC -promoting survival or inducing death -is the central question that this study seeks to answer. TNBC cells are often in a state of high ERS due to rapid proliferation and a high protein load (Zhang *et al*., 2024). Moderate ER-phagy helps remove damaged ER and misfolded proteins, thereby maintaining cellular homeostasis (Amano *et al*., 2025; Dutheil *et al*., 2025). However, in the present study, everolimus significantly upregulated ER-phagy receptors (FAM134B increased by 4.32-fold) via TFEB, leading to an abnormal increase in ER-phagy flux and ultimately triggering cell death, with the apoptosis rate rising from 6.2% to 34.7%. In the mCherry-GFP-KDEL reporter assay, ER transport to lysosomes was significantly increased. Electron microscopy directly observed the typical structure of endoplasmic reticulum autophagic vesicles. These results suggest that there may be a "protective threshold" of ER-phagy in TNBC cells:

Article in Press

moderate ER-phagy is required for survival, but is exceeded by TFEB-driven hyperactivation, shifting ER-phagy from an adaptive mechanism to an irreversible lethal event. This model of "excessive autophagy leading to cell death" is consistent with the clinical observation of previous studies (Koizumi and Ono,2025), who observed that LC3B-positive areas accounted for 32.50% of the total thrombus area in patients with everolimus-coated stent implantation, suggesting that everolimus can induce excessive autophagy-related damage in normal tissues.

The main role of FAM134B

Of the three ER-phagy receptors examined in this study, FAM134B was the only one whose knockdown significantly reversed the cytotoxic effects of everolimus. After FAM134B knockdown, everolimus-induced ER autophagic vesicles decreased from 5.79 to 0.46; the proportion of swollen ER cells decreased from 77.36% to 7.85% and cell viability increased from 22.45% to 78.92%. Complementation of FAM134B could re-enhance the killing effect of everolimus. These results indicate that FAM134B is an indispensable major downstream effector molecule in this pathway. FAM134B is a known ER-phagy receptor that binds to LC3 via the LIR motif and mediates endoplasmic reticulum bending and fragmentation (Najafizade *et al*., 2025; Gatica *et al*., 2025). This study identifies FAM134B as a key downstream target of the mTORC1/TFEB axis, providing a novel functional anchor for this pathway in TNBC. Meanwhile, RTN3L and CALCOCO1 are also transcriptionally regulated by TFEB, suggesting the possibility of functional redundancy or tissue-specific compensatory mechanisms, whose exact contributions require further investigation.

Clinical translational significance and limitations

The findings of this study have potential translational clinical implications. In the TNBC subset with high FAM134B expression, everolimus alone may be sufficient to induce lethal ER-phagy. However, in those with low FAM134B expression, combination with ER-phagy inducers or ERS agonists may enhance drug sensitivity. Previous clinical studies (Tan *et al*., 2025) showed that 22.33% of TNBC patients with a non-luminal disease score (including Ki-67 ≥ 30%, histological grade 3, tumor size > 5 cm, etc.) ≥ 3 points had a PFS of only 2.10 months with everolimus. Whether FAM134B expression levels can provide a more accurate prediction of efficacy. However, it must be emphasized that this study has been conducted in only two TNBC cell lines and one xenograft model. TNBC is highly molecularly heterogeneous and these findings cannot be directly generalized to all TNBC patients. In addition, nonmalignant breast epithelial cells were not included as controls, so it is unclear whether the everolimus-induced ER-phagy hyperactivation is selective for tumor cells. This study also did not use patient-derived samples, organoids, or primary cells for validation; the clinical translational credibility still needs further evidence.

Unresolved issues and future directions

Some questions remain unanswered in this study. In addition to mTORC1, TFEB is regulated by other kinases, such as MAPK, AKT and GSK3β. Whether everolimus indirectly affects TFEB through the above pathways remains to be tested. Second, there is currently evidence of a correlation between TFEB nuclear localization and increased expression of ER-phagy markers. A direct causal link requires further verification by conditional gene knockout experiments. In addition, the temporal relationship and causal link between everolimus-induced overactivation of ER-phagy and apoptosis still need to be confirmed by more refined time-course experiments. Third, the present study reveals a critical role for FAM134B in everolimus-induced cell death, but whether the regulation of RTN3L and CALCOCO1 exerts a compensatory function under certain conditions warrants further exploration. Finally, the clinical value of FAM134B as a predictive biomarker for efficacy needs to be prospectively validated in an independent clinical cohort.

CONCLUSION

In summary, the present study systematically characterized the signaling pathway by which everolimus activates ER-phagy and induces cell death via the mTORC1/TFEB/FAM134B axis in TNBC cells and xenograft models. This finding provides a new mechanistic perspective on the limited single-agent activity of mTORC1 inhibitors in TNBC and an experimental basis for future optimization of combination therapy strategies and exploration of potential biomarkers.

Acknowledgments

This work was supported by the Guiding Project of the Nanjing City Health Science and Technology Development Special Fund for the Year 2025 (Grant No. ZDXX25140).

Authors' contributions

Xia Da: Conceptualization (lead), methodology (equal), investigation (lead), data curation (equal) and visualization (equal); Bin Zhang: Conceptualization (supporting), writing – original draft (lead), funding acquisition (lead) and project administration (equal); Jin Lv: Investigation (supporting), data curation (lead), formal analysis (lead) and validation (equal); Jin Xu: Conceptualization (supporting), supervision (lead), writing–review and editing (lead), resources (lead) and project administration (lead). All authors participated in data interpretation and manuscript revision and agreed to the submission and publication of the final version.

Article in Press

Funding
This work was supported by the Guiding Project of the Nanjing City Health Science and Technology Development Special Fund for the Year 2025 (Grant No. ZDXX25140).

Data availability statement
The datasets generated during and/or analyzed during the current study are available from the corresponding author upon reasonable request.

Ethical approval
This study was conducted in accordance with the Declaration of Helsinki and the guidelines of the Institutional Review Board. The animal experimental protocol was approved by the Institutional Animal Care and Use Committee of Nanjing First Hospital, Nanjing Medical University (Approval No.: KY20260112-KS-08). All animal procedures strictly followed the NIH Guide for the Care and Use of Laboratory Animals (8th edition, 2011) and were reported in compliance with the ARRIVE guidelines. Human cell lines used in this study were obtained from ATCC and did not involve human subjects or clinical samples. Thus, no additional human ethics approval was required. This study was performed in adherence with the ARRIVE guidelines. See supplementary file for the ARRIVE checklist.

Conflict of interest
The authors declare no conflict of interest.

REFERENCES

Akayama S, Shima T, Kaminishi T, Cui M, Monfregola J, Nishino K, Ballabio A, Kosako H, Yoshimori T and Nakamura S (2025). ATG conjugation-dependent/ independent mechanisms underlie lysosomal stress-induced TFEB regulation. *J. Cell Biol*., **224**(10): e202307079.

Alkassis S, Suresh Y, Lipsyc-Sharf M, Zhang S, Gianni C, Medford A, Bardia A, Ashouri S and Kapoor N (2025). Circulating tumor DNA detection of local recurrence in a patient with early stage triple-negative breast cancer. *Breast Cancer Res. Treat*., **213**(2): 219-223.

Amano Y, Tanino R, Sun R, Tsubata Y, Isobe T and Okimoto T (2025). Inhibition of small-cell lung cancer angiogenesis by irinotecan metronomic chemotherapy and irinotecan plus everolimus. *Anticancer Res*., **45**(12): 5287-5297.

Demirkesen S, Iriagac Y, Seber ES and Aral C (2025). Melatonin enhances everolimus efficacy in breast cancer by suppressing mTOR pathway activation and promoting apoptosis and mitochondrial function. *BMC Pharmacol. Toxicol*., **26**(1): 100.

Dias D, Oliveira E, Marti-Diaz R andrews S, Chocarro-Calvo A, Bellini A, Mosteo L, Garcia YV, Chauhan J, Li L, Garcia-Martinez JM, Rodriguez-Lopez JN, Maria-Engler SS, Kenny C, Martinez-Useros J, Garcia-Jimenez C, Sanchez-Del-Campo L, Louphrasitthiphol P and Goding CR (2025). MITF, TFEB and TFE3 drive distinct adaptive gene expression programs and immune infiltration in melanoma. *Cell Rep*., **44**(12): 116499.

Dutheil J, Pereira V, Boisson C, Mansi L, Paillard MJ, Bazan F, Chaigneau L, Dobi E, Viot J, Meynard G, Goujon M, Dalens L, Dubourd C, Marchi S, Meneveau N, Vernerey D, Adotevi O, Meurisse A and Curtit E (2025). Efficacy of everolimus in patients with hormone receptor positive, HER2 negative, metastatic breast cancer pretreated with CDK4/6 inhibitors. *Breast Cancer Res*., **27**(1): 220.

Fan L, Wang ZH, Ma LX, Wu SY, Wu J, Yu KD, Sui XY, Xu Y, Liu XY, Chen L, Zhang WJ, Jin X, Xiao Q, Shui RH, Xiao Y, Wang H, Yang YS, Huang XY, Cao AY, Li JJ and Shao ZM (2024). Optimising first-line subtyping-based therapy in triple-negative breast cancer (FUTURE-SUPER): A multi-cohort, randomised, phase 2 trial. *Lancet Oncol*., **25**(2): 184-197.

Gatica D, Alsaadi RM, El Hamra R, Li B, Mueller R, Miyazaki M, Sun Q, Sad S and Russell RC (2025). The ER-phagy receptor FAM134B is targeted by *Salmonella typhimurium* to promote infection. *Nat. Commun*., **16**(1): 2923.

Khadiri K, Khadrouf Z, Sadry M, Essalihi A, Bouchra O, Benchekroun MT and Karkouri M (2026). Locoregional recurrence of triple-negative breast cancer with low tumor-infiltrating lymphocytes: A case report. *Pan. Afr. Med. J*., **52**: 161.

Koizumi T and Ono M (2025). Late stent thrombosis after biodegradable polymer everolimus-eluting stent in a cancer patient receiving bevacizumab. *JACC Case Rep*., **30**(35): 105597.

Liao F, Yang W, Shi J, Peng Y, Wang J, Li H, Tan L, Long L, Fu C and Qu H (2026). Huoxue Jiedu formula attenuates myocardial ischemia-reperfusion injury by modulating LAPTM4B/mTORC1/TFEB pathway-mediated autophagic flux. *Phytomedicine*., **157**: 158306.

Licata L, Mariani M, Viale G, Dent R, Tolaney SM, Schmid P, Hamilton E, Sotiriou C, Pusztai L and Bianchini G (2025). Timing of recurrence after neoadjuvant chemo-immunotherapy in patients with early-stage triple-negative breast cancer. *Clin. Cancer Res*., **31**(18): 3916-3921.

Mehlich D and Marusiak AA (2022). Kinase inhibitors for precision therapy of triple-negative breast cancer: Progress, challenges and new perspectives on targeting this heterogeneous disease. *Cancer Lett*., **547**: 215775.

Nafissi N, Mahadevan A, Chiao E, Rijal N and Parajuli R (2026). Triple negative breast cancer with choroidal metastasis responsive to sacituzumab govitecan and radiation therapy. *Cancer Rep*., **9**(2): e70462.

Najafizade N, Zarei S, Elhaie M and Roayaei M (2025).

Article in Press

Comparative efficacy of palbociclib and everolimus with aromatase inhibitors in second line treatment of HR and HER2 negative metastatic breast cancer. *Discov. Oncol*., **17**(1): 150.

Negoita F, Fraguas Bringas C, Hellberg K, Luda KM, Liu H, Li Z, Cuenco J, Zhao JF, Sathe G, Ganley IG, Sapkota GP and Sakamoto K (2026). AMPK promotes TFEB transcriptional activity through dephosphorylation at both MTORC1-dependent and -independent sites. *Autophagy*., **22**(6): 1386-1400.

Patel R, Fukui J, Klein P, Moshier E, Kocyigit H, Fiedler L, Bucwinska W, Xing XY, Shapiro C, Goel A, Fasano J, Shao T, Bhardwaj A, Kim E, Vaccaro R, Lee K, Wilck E and Tiersten A (2025). Randomized phase II comparison of single-agent carboplatin versus combination of carboplatin and everolimus for advanced triple negative breast cancer. *Breast Cancer Res Treat*., **214**(2): 159-170.

Polho GB, Shinkado YR, Murazawa LK, Oliveira VV, Pinheiro VR, Labanda DDCP, Barroso-Sousa R, Carvalho Barros LR, Testa L and Bonadio RC (2025). Reply letter: Pathologic complete response in TNBC: A shield against recurrence, but not the brain? *Breast*., **84**: 104605.

Rota S, Sciortino C, Damian S, Duca M, Villa G, De Monte M, Ebrahem E, Cattaneo L, Volpi C, Casale A, Sorrentino D, Pessina S, Martinetti A, De Braud F and Cresta S (2025). ICIs exceptional long response in TNBC: Addressing the issue of optimal ICIs duration. Two cases and review of the literature. *Cancer Rep*., **8**(11): e70397.

Shang Y, Si W, Zhang Y, Liu J, Zhang H, Li Y, Su H, Jiang W, Ding Z and Wang L (2026). Tetrastigma hemsleyanum polysaccharide suppresses triple-negative breast cancer by disrupting the Hippo-YAP/TEAD4-PDIA4 axis and endoplasmic reticulum stress adaptation. *Adv. Sci*., **13**(34): e19006.

Soleimani M, Duchow M, Goyal R, Somma A, Kaoud TS, Dalby KN, Kowalski J, Eckhardt SG and Van Den Berg C (2025). Transcription factor EB (TFEB) activity increases resistance of TNBC stem cells to metabolic stress. *Life Sci. Alliance*., **8**(3): e202302259.

Tan Y, Jiang H, Tian X, Ma F, Wang J, Zhang P, Xu B, Fan Y and Zhao W (2025). Non-luminal disease score for everolimus in patients with hormone receptor-positive and human epidermal growth factor receptor 2-negative advanced breast cancer: A multicenter and retrospective study. *Breast Cancer*., **17**: 67-78.

Valachis A, Geisler J, Karihtala P and Tuxen MK (2026). Insights on postneoadjuvant treatment among patients with triple-negative breast cancer and residual disease after neoadjuvant therapy: can expert consensus help to interpret the current evidence? *Br. J. Cancer*., **135**(3): 329-335.

Wang J, Xu H and Tang L (2025a). Targeting TDP-43-activated GRP78/endoplasmic reticulum stress axis suppresses triple-negative breast cancer progression. *Biochem. Pharmacol*., **242**(Pt 2): 117331.

Wang PH, Yang ST and Kuo TC (2025b). Outcomes of everolimus-treated HR+/HER2- breast cancer. *J. Chin. Med. Assoc*., **88**(10): 730-732.

Zhang Y, Wang H, Zhu L, Chen X, Zhao M and Liu M (2025a). Construction and validation of predictive model based on endoplasmic reticulum stress-related genes for triple-negative breast cancer. *Cell Cycle*., **24**(17-20): 350-371.

Zhang M, Xu J, Liu Q, Yan X and Li N (2025b). TROP2 regulates cisplatin sensitivity of triple-negative breast cancer cells by regulating endoplasmic reticulum stress. *Histol. Histopathol*., **40**(2): 259-268.

Zhang D, Chen H, Wang J, Ji J, Imam M, Zhang Z and Yan S (2024). Current progress and prospects for G protein-coupled estrogen receptor in triple-negative breast cancer. *Front. Cell Dev. Biol*., **12**: 1338448.

Zhao D, Song J and Ji C (2025). Endoplasmic reticulum stress regulates apoptosis and chemotherapeutic via enhancing TNFRSF10B recycling to the cell membrane in triple-negative breast cancer. *Clin. Transl. Oncol*., **27**(1): 265-276.

Article in Press